# Power Quality Measurements in a Low-Voltage DC Microgrid in an Open Parking Garage

H. E. van den Brom
VSL, National Metrology Institute
Delft, the Netherlands
hvdbrom@vsl.nl

R. van Leeuwen
VSL, National Metrology Institute
Delft, the Netherlands
rvanleeuwen@vsl.nl

J. M. Warmerdam
Faculty of Technology
Amsterdam University of Applied Sciences
Amsterdam, the Netherlands
j.m.warmerdam@hva.nl

R. Schaacke
Faculty of Technology
Amsterdam University of Applied Sciences
Amsterdam, the Netherlands
r.schaacke@hva.nl

***Abstract*—Low-voltage DC microgrids are becoming more widely acknowledged as a viable option as local extensions of the conventional AC distribution grid. Consequently, consistent definitions and measuring techniques of the parameters and criteria defining the power quality of these DC microgrids are needed, analogous to the traditional standards for AC electricity. An open issue in this aspect is the lack of available measurement results in real-world situations. In this paper, the results of a power quality measurement campaign performed in a unipolar 700 V DC microgrid in an open parking garage with currents up to 35 A are presented.**

***Keywords—DC Microgrid, DC Power Distribution, Fourier Analysis, Low-Voltage DC grid, measurement, Power Quality, Ripple, Standardization***

## I. Introduction

With the increasing generation, use, and storage of distributed energy, local DC grids are becoming an attractive addition to traditional AC distribution networks. Most electronic devices, including sustainable technologies such as LED lighting, photovoltaic (PV) cells, and electric vehicles (EVs), basically use direct current (DC) and need power conversion when connected to the conventional alternating current (AC) grid. Therefore, connecting these electronic devices to local low-voltage (LV) DC microgrids avoids the excessive use of converters and their related energy losses [1].

A lot of research has been performed already on LV DC microgrids, focusing on control and stability [2], system architecture [3], and planning and implementation issues [4]. Measurements in real DC trial grids have been reported as well, investigating the power flow [5], energy management and harmonics [6], and efficiency, losses, and potential energy savings [7].

AC grids are very well regulated and standardized already. With the increasing attractiveness of DC microgrids, the need for standardizing DC power systems is increasing as well. The focus of standardization activities for DC grids is currently on installation, safety, voltage levels, and fault detection [8]. However, like AC grids, DC microgrids must fulfill power quality (PQ) limits to guarantee reliable operation as well. Knowledge about PQ events and phenomena occurring in public DC systems is currently lacking, and so are the related measurement techniques. DC PQ issues differ from those in AC systems because different electronics are involved and, more fundamentally, switching in DC leads to higher voltage transients due to the missing repetitive zero-crossings that intrinsically happen in AC power systems. Furthermore, harmonics caused by rectifiers in AC-DC converters linking the DC grid to the AC distribution system can enter the DC microgrid and might cause malfunctioning of equipment and component heating.

Power quality in DC systems is fundamentally different from AC due to the lack of a fundamental frequency. Therefore, for instance, harmonics, interharmonics, and supraharmonics cannot be defined, and need to be replaced by another metric. Furthermore, there is no natural timescale for averaging measurement results, such as the half-cycle in AC. Also, DC power systems operating in islanding mode have much lower inertia than conventional AC systems, whereas the voltage stability is defined by power curtailment systems and droop control mechanisms that are based on voltage control rather than on frequency control as in AC systems, resulting in voltage levels that are much less stable than those for AC systems. Several definitions of DC PQ indices and statistical indicators have been proposed in the meantime [9] and standardization is starting slowly [10] but is hampered by a lack of measurement data in real DC grids in practice. Initial measurement results are available for DC railway systems [11], but results from other types of DC grids are necessary as well. Pending the measurement results in other DC grids, considerations on the detection of dips, swells, and interruptions [12] and voltage ripple [13] for DC electricity grids were presented already, based on the preliminary analysis of measurements in DC railway systems.

The need for measurements to underpin new definitions of DC PQ is addressed in the European metrology project "20NRM03 DC Grids" [14] by measuring and analyzing the distortions occurring in LV DC microgrids and developing reference systems for the calibration of DC power meters [15] and DC PQ analyzers, and for testing DC equipment such as DC electricity meters in the presence of well-defined distortions [16]. The first measurement campaigns have been executed already in LV DC microgrids in Malaga Smart City in Spain, with micro wind turbines and PV panels at a voltage level of 48 V [17], the Green Village in Delft, the Netherlands, with LED streetlights and PV panels and operated at 350 V [18], and three different public EV charging stations in Germany [19].

In [18], different definitions of DC voltage and current distortions were investigated for a real-world LV DC microgrid, and recommendations were given, in particular for

The research leading to the results described in this paper is performed within the project 20NRM03 "DC grids" of the European Metrology Programme for Innovation and Research (EMPIR). The EMPIR initiative is co-funded by the European Union's Horizon 2020 research and innovation programme and the EMPIR participating states. Additional funding was received from the Dutch Ministry of Economic Affairs and Climate Policy.

the ripple content and frequency components, including the influence of the selection of the time window and the frequency resolution on these parameters. However, the power flow in the microgrid investigated in that study was rather low, and information on the magnitude of the distortions for microgrids with higher levels of power flow and other power electronics such as EV chargers connected is still missing.

This paper presents the measurement results obtained during a measurement campaign in a DC grid installed in an open parking garage in Utrecht, with PV panels, EV chargers, and LED lighting, operating at 700 V. In the next section, the DC grid under investigation is presented and the measurement system and measurement procedure are explained. In subsequent sections, the measurement results are analyzed and discussed following the recommendations of [18] and conclusions are drawn.

## II. Experimental procedure

### A. Description of the DC microgrid

The LV DC grid investigated in this paper is installed in an open parking garage in Utrecht, the Netherlands, located at the headquarters of the insurance company A.S.R., which is designed to be a highly sustainable building. The grid is operated at a unipolar voltage of nominally 700 V and is connected to the 400 V AC distribution grid through a single active front end that serves as a galvanically isolated bidirectional AC-DC interlink converter balancing the load and supply. A capacitor of 4000 µF is connected between the positive and negative wires at the DC side of the converter to be able to quickly respond to sudden changes in the system. The microgrid can be operated in grid-connected or islanding mode by disconnecting the interlink converter. Six strings of 14 solar PV panels, i.e., 84 panels in total, of the type DMEGC 435Wp, typically delivering a power of 10 kW in total, are connected to the DC grid through three maximum power point trackers (MPPTs). Three bidirectional EV chargers, each delivering 10 kW maximum, are connected to the main bus through a single conductor. The EV chargers are provided with CHAdeMO and Combined Charging System (CCS) connectors, and the charging power can be set through dedicated operating software. LED lighting for the parking places at the EV chargers is fed by the same DC grid as well. Droop rate control mechanisms have been installed with voltage and power settings for each device. Current routers using solid-state switching ensure ulta-fast breaking in case of faults. Furthermore, a separate safety wire controls all sources connected to the microgrid, i.e., if the independent 48 V signal of the safety wire is lost, all sources will discontinue supplying power to the DC bus. The earthing configuration facilitates the determination of current leakage using separate DC stray current sensors embedded in the concrete structure to minimize corrosion. A diagrammatic overview of the grid is presented in Fig. 1.

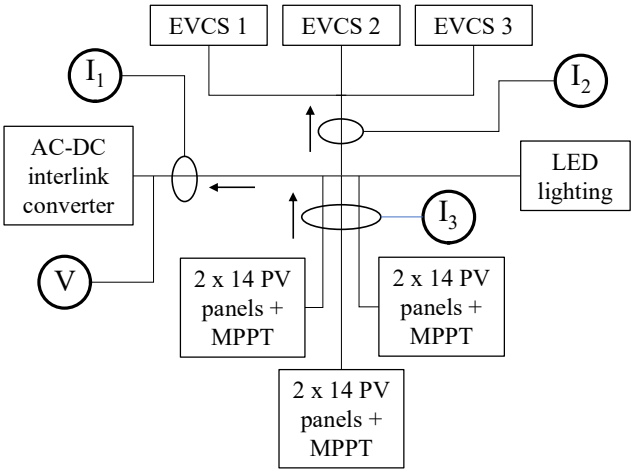


Fig. 1. Diagrammatic representation of the positive polarity conductors of the LV DC microgrid under investigation, with the AC-DC link to the AC distribution grid, the MPPTs regulating the PV power, the EV charging stations, the LED lighting, and the installed voltage and current sensors. The negative polarity conductors, and, consequently, the capacitor between the positive and negative wires at the output of the converter are not shown. The arrows show the direction of positive currents through the sensors.

### B. Measurement equipment

The measurement equipment used in the experiments described here is similar to the one used in [18]. For the voltage measurement, a Hioki type 9322 transducer was used, which is a 2 kV, 1 mV/V, 10 MHz differential voltage probe; the bandwidth was limited to 500 kHz using a low-pass filter for reasons explained below. The current at the point of connection at the AC-DC interlink converter and the current to and from the EV charging stations is measured using two Hioki type CT6843-05, 200 A, 10 mV/A, 500 kHz openable-core high-accuracy zero-flux current sensors. The current from the three groups of PV panels is measured simultaneously using a Hioki type CT6862-05, which is a 50 A, 40 mV/A, 1 MHz AC/DC pass-through high-precision zero-flux current sensor, i.e., the current sensor encloses all three connecting conductors.

Further investigation of the time traces of the measurement data in previous measurements [18] sometimes showed spiky distortions with significant amplitude, consisting of only one single sample. This indicates the potential high-frequency pickup or infeed of signals at frequencies beyond the bandwidth of the digitizer but within the bandwidth of the voltage sensor. Therefore, for the measurements described in this paper, the voltage input is provided with an analog anti-aliasing filter, which is a passive two-stage low-pass filter with a cut-off frequency of around 500 kHz, which is equal to the Nyquist frequency when sampling with 1 MSa/s. The two stages of the filter were both realized with a 1 nF capacitor in combination with a 330 Ω metal film resistor. In order to improve the quality of the filter, two different types of capacitors were used, i.e., one metalized polyester film capacitor and one ceramic capacitor. Testing of the filters indeed showed a suppression of the spikes to levels lower than those of the other noise.

The output of the voltage and current sensors is recorded using a waveform recorder originally designed for AC applications [20] but adapted for use in DC grids. It is based on a Picoscope 4824 oscilloscope, which is an 8-channel, 12-bit, 20 MHz digitizer. The output signals of the sensors were sampled with a sampling rate of 1 MSa/s. A minicomputer is built in for running the data acquisition software, whereas an external solid-state drive is connected for local storage of the raw measurement data. The raw data were stored in files consisting of subsequent and gapless 1-second windows, which resulted in hundreds of GB of data after a few hours of measurements. To avoid losing valuable information, rather than exploiting trigger mechanisms to reduce the massive amount of measurement data [17], it was decided to store all sampled data unconditionally to be investigated afterward for

the presence of distortions, because a priori there is no clear indication of the type and magnitude of the distortions present in this DC microgrid.

The uncertainties of the voltage sensor at 700 V, the current sensors at 10 A, and the waveform recorder input channels in the 1 V range, as determined using a method similar to the one presented in [21], are within 0.1 % over the entire frequency range of interest up to 150 kHz. To investigate what types of PQ phenomena occur in LV DC microgrids and what are their typical magnitudes, this uncertainty is more than sufficient.

### C. Measurement procedure

The voltage $V$ and current $I_1$ at the point of connection of the AC-DC interlink converter and the current from the EV charging stations $I_2$ and the PV system $I_3$ were recorded continuously with a sampling rate of 1 MSa/s. The measurements were performed in the afternoon of a partially cloudy day with sunshine at the end of September. Therefore, the solar energy supplied to the system varied with the clouds covering the sun. Several different situations were investigated, including EV charging in grid-connected mode and in islanding mode (i.e., with the link to the AC grid disconnected), the solar panels feeding the AC grid in the absence of EV charging, and an EV feeding the grid when discharging. Two different EVs were subsequently connected to one of the EV charging stations when measuring, that is, a Hyundai Ioniq with a CCS connector and a Nissan Leaf with a CHAdeMO connector. The EV charging power was controlled using software; typically 5 kW, 7 kW, or the maximum of 10 kW was used.

## III. Ripple Content: Measurements and Discussion

### A. Measurand definitions

In the absence of a fundamental frequency, harmonics, interharmonics, and supraharmonics cannot be defined, but repetitive distortions can still be quantified by their variation around an averaged DC value and their spectral components.

The data from the four measurement channels is represented by four sets of samples $\{x_i\}$, $i$ being the sample number. These sets represent the bus voltage $V$ and the three currents, $I_1$, $I_2$, and $I_3$, as indicated in Fig. 1. For each of these datasets, the average values

$$x_{\mathrm{DC}} = \frac{1}{N}\sum_{i=0}^{N-1} x_i \qquad (1)$$

and the root-mean-square (RMS) values

$$x_{\mathrm{RMS}} = \sqrt{\frac{1}{N}\sum_{i=0}^{N-1} {x_i}^2} \qquad (2)$$

were determined for each subsequent 1-second time window, where $N = 1{,}000{,}000$ is the number of samples per time window.

The ripple content was determined from (1) and (2) as

$$x_{\mathrm{ripple}} = \sqrt{{x_{\mathrm{RMS}}}^2 - {x_{\mathrm{DC}}}^2}\,. \qquad (3)$$

The ripple content defined this way is a measure of the total contribution of the spectral content of the signal $x_i$ in each 1-second time window beyond the DC component, i.e., including noise and electromagnetic interference; in fact, it is equivalent to the standard deviation of a random variable $x$. Different definitions of ripple and time windows have been considered [13] and applied to real measurement data [18] before; for the purpose of this paper, we only consider the RMS-based definition of ripple in (3) and fix the time window to 1 second.

### B. Measurement results

An example of the raw voltage data during a 1-second time window corresponding to the initiation of the charging process of an EV is presented in Fig. 2. The ripple content and DC values of the voltage, and the ripple content and DC values of the current at the AC-DC interlink converter, the EV charging stations, and the PV system, calculated for each successive 1-second time window using (1) and (3), are presented in Fig. 3. The magnitudes of the ripple are shown on the left vertical axes, the DC values are shown on the right axes. The signs of the DC current values correspond to the current directions indicated in Fig. 1. The vertical scales are adjusted such that the range of interest of the measurands is properly indicated and the gridlines of the left and right axes coincide. Consequently, the highest peak values of the ripple content are not visible. Furthermore, the time axis is cropped after time $t = 9000$ s because after that no events or other phenomena of particular interest occurred.

### C. Observations

The DC voltage in Fig. 3 typically shows variations between 685 V and 750 V. The microgrid was in grid-connected mode between $t = 1800$ s and $t = 4200$ s and after $t = 6100$ s; before $t = 1800$ s and between $t = 4200$ s and $t = 6100$ s it was in islanding mode. As can be seen, in grid-connected mode the voltage was between 685 V and 725 V, which is lower than in islanding mode, where it was between 730 V and 750 V. The zero voltage values only occurred when intentionally switching off the system or when the EV charging power was set too high in islanding mode and the PV system could not keep the voltage sufficiently high, causing the system to automatically switch off (which occurred twice around $t = 800$ s and once around $t = 4400$ s).

The corresponding voltage ripple content shows more or less stable values between 0.65 V and 0.8 V, accompanied by many large peaks. First of all, it should be mentioned that these more or less stable values are almost two orders of magnitude lower than the values observed in [18]. This is most likely due to the bandwidth being strongly reduced by the low-pass filter to suppress the aliasing of high-frequency electromagnetic interference and noise. Furthermore, the more or less stable ripple values correspond to quasi-static situations, in which the voltage and current remain stable within the 1-second time window over which the ripple is calculated. However, if the voltage or current changes within the 1-second window, for instance, due to the onset of the EV charging process (as illustrated in Fig. 2) or variations in solar power, the difference between the RMS value of (2) and the DC value of (1), which is the ripple value of (3), will become large, similar to calculating the standard deviation of a non-stationary signal. Hence, the observed peaks in the ripple content are due to changes in the system rather than caused by increased quasi-stationary distortions.

The DC current values of the EV chargers were observed to be positive as well as negative because the EV can either be charged or uncharged. As expected, the PV current only has positive values. Between $t = 2100$ s and $t = 2700$ s the PV current unfortunately clipped at 25 A due to the voltage range setting of the waveform recorder. Typically, the current

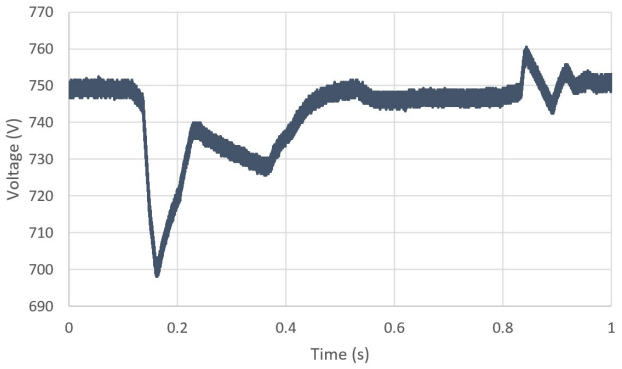


Fig. 2. Example of voltage samples during a 1-second time window corresponding to the starting of the charging process of an EV.

measured at the EV charging stations, both when charging an EV or when an EV is feeding the microgrid, is on the order of 10 A to 15 A, which is similar to the current from the PV system, depending on the amount of solar irradiation. The latter can, for instance, be seen above $t = 6100$ s in the lowest graph of Fig. 3, when the PV system was feeding the AC grid and hardly any power was consumed, such that approximately the same current was measured at the interlink converter (second graph in Fig. 3).

The current ripple content shows large fluctuations for the PV system, which is particularly clear between $t = 2100$ s and 2700 s and above $t = 6100$ s. In the case of the $t = 2100$ s to $t = 2700$ s band, the clipping mentioned above partially obscures the ripple observations because the ripple is zero when the sensor clips, even though the actual ripple content is high. Another observation is that the current ripple content at the interlink converter is approximately 10 times higher than the ripple at the EV charging stations or the PV system, and much less fluctuating than the ripple at the PV system. The latter is even the case in the period after $t = 6100$ s when the current through the interlink converter is mainly defined by the PV current that is fed directly to the AC grid. This suggests that the interlink converter is the main cause of the distortions.

## IV. Spectral Analysis

### A. Measurand definition

Since the ripple content only provides information on the magnitude of all frequency components combined, the spectral content of each 1-second window was investigated as well. For this purpose, the Discrete Fourier Transform (DFT)

$$X_k = \frac{1}{N}\sum_{i=0}^{N-1} x_i \cdot e^{-\frac{j2\pi}{N}k\cdot i} \qquad (4)$$

was calculated for each time window, $k$ representing the frequency. The electrical engineering convention of a normalization factor of $1/N$ in the DFT itself rather than in its inverse is chosen such that the $k = 0$ component is equal to the DC value defined in (1).

For frequencies up to 2 kHz, a frequency resolution of 5 Hz was used, in line with the AC PQ harmonic analysis defined in the IEC 61000-4-7. To reduce the calculation time, for frequencies between 2 kHz and 150 kHz, the resolution was limited to 200 Hz, as suggested in the IEC 61000-4-30. Therefore, each window was divided into 200 ms or 5 ms sub-windows, respectively. The resulting 5 or 200 DFTs, respectively, were averaged such that one single DFT

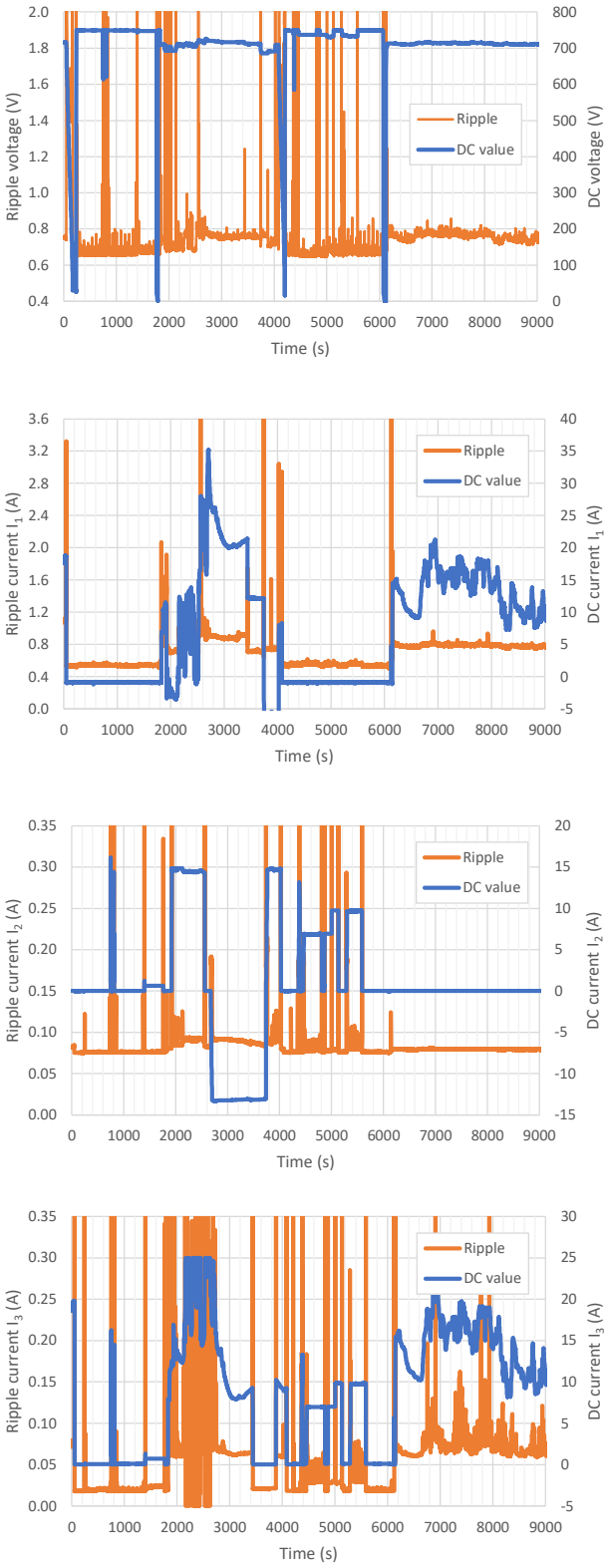


Fig. 3. From top to bottom: ripple content (left vertical axis) and DC value (right vertical axis) of the voltage signal $V$ and the current $I_1$ at the AC-DC interlink converter, the current $I_2$ at the EV charging stations, and the current $I_3$ at the PV system, respectively.

characterizes the whole 1-second time window. Note that since the frequency components of the ripple content are not known a priori, and, in particular, are not necessarily integer multiples of 50 Hz but can have any frequency, the sub-windows do not necessarily contain an integer number of

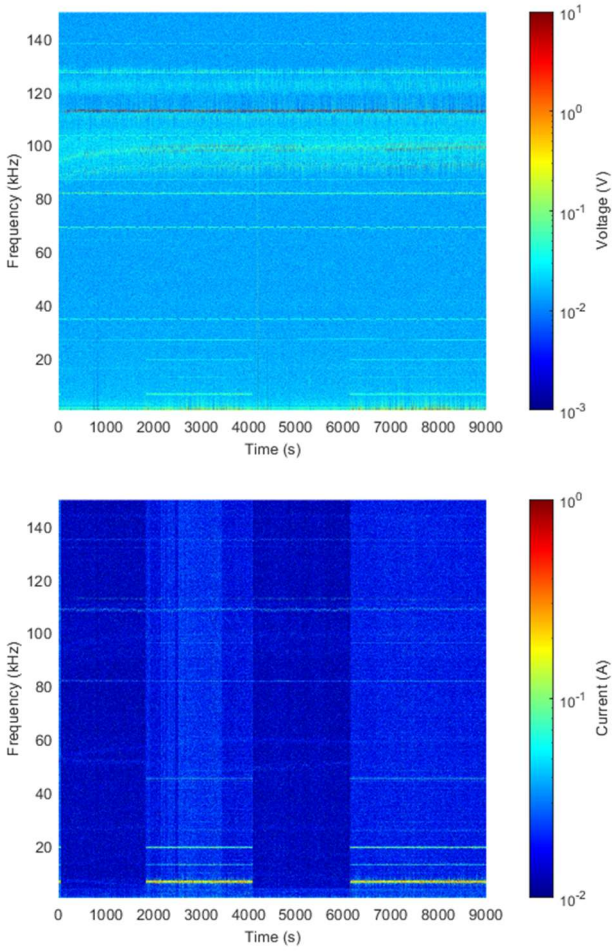


Fig. 4. DFTs of the voltage signal $V$ (upper graph) and the current $I_1$ (lower graph) at the AC-DC interlink converter in the frequency range up to 150 kHz.

cycles, and part of the power contained in the peaks can leak into side lobes, thus lowering the actual value of the peak. However, for the goal of this paper, which is to identify the general features of the ripple content, this is sufficient.

### *B. Measurement results*

Apart from DC values and ripple content, the corresponding DFTs were calculated for each 1-second time window using (4). The procedure explained in Section IV-A was followed to produce separate graphs for the frequency ranges up to 150 kHz with a resolution of 200 Hz and up to 2 kHz with a resolution of 5 Hz, respectively.

The DFTs of the voltage and current at the AC-DC interlink converter are presented as two-dimensional (2D) density charts for frequencies up to 150 kHz in Fig. 4, in which the magnitudes are indicated using the color bar. The measurement results for the other current sensors look similar but do not add much to the present paper. The DFTs of the voltage signals are presented in Fig. 5 for frequencies up to 2 kHz. The DFTs of the current signals below 2 kHz did not show any significant peaks above the noise background and are not presented in Fig. 5.

### *C. Observations*

The spectral components of the voltage signal at frequencies above 20 kHz as presented in Fig. 4 show persistent maxima over the entire time frame, independent of the configuration or loading, indicating pickup or infeed of

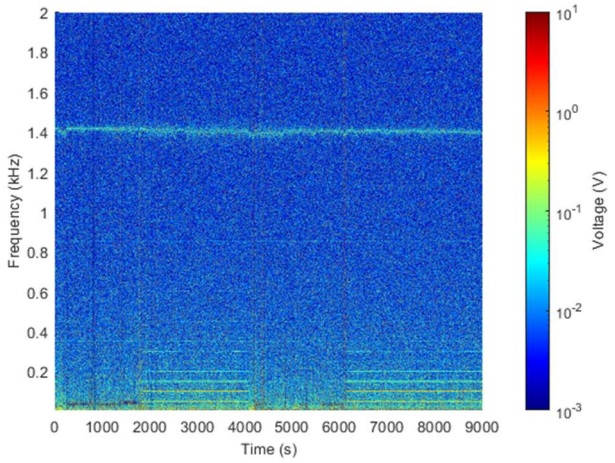


Fig. 5. DFTs of the voltage signal $V$ at the AC-DC interlink converter in the frequency range up to 2 kHz.

electromagnetic interference. Since the frequency components differ from the spectra observed in [18], these spectra are related to the particular microgrid and not due to the measurement equipment. It should be noted that the persistent peak just below 100 kHz is slowly changing its frequency, suggesting some kind of warm-up or switch-on effect, even though all equipment was operational at least for several hours already. At frequencies below 20 kHz, the occurrence of maxima coincides with the increased level of ripple in grid-connected mode, i.e., between $t = 1800$ s and $t = 4200$ s and after $t = 6100$ s, as was observed in Fig. 3.

For the lowest frequencies, Fig. 3 shows that within the resolution of 5 Hz, the frequencies of the maxima observed in grid-connected mode are integer multiples of 50 Hz, with a highest peak at 100 Hz. This suggests that the rectifiers in the AC-DC interlink converter are the main cause of the distortions. This is different from the spectra discussed in [18], where the low-frequency distortions contained frequency components that were not an integer number of 50 Hz and might for instance be caused by the control mechanisms of the MPPTs in the grid investigated. A persistent maximum at a frequency of around 1.4 kHz can also be observed. Note that the choice of the normalization factor of $1/N$ in (4) causes the DFT values of a white noise signal to scale with $1/\sqrt{N}$, which explains the difference in background noise observed in Fig. 5 and in the upper graph of Fig. 4 (which use the same color scaling).

In general, the current ripple seems to follow the voltage ripple. However, although generally speaking the frequencies of the observed maxima coincide, the highest magnitudes for the current signals mainly show up at lower frequencies, i.e., around 7 kHz, whereas for voltage they occur at significantly higher frequencies, i.e., around 113 kHz.

## V. Summary and Conclusions

In this paper, the results of a measurement campaign obtained in a unipolar 700 V DC microgrid in an open parking garage are presented. Voltage and current signals were registered continuously at the AC-DC interlink converter, EV charging stations, and PV panels. During the measurements, the configuration of the microgrid was changed to investigate different situations, such as EV charging and discharging or grid-connected and islanding mode.

The measurements were taken with metrology-sound measurement equipment that was developed specifically for this purpose. The voltage and current signals were recorded during the whole 4-hour measurement period with a sampling rate of 1 MSa/s. The resulting measurement data were stored locally and analyzed afterward using 1-second time windows, with a focus on DC voltage and current variation, ripple, and spectral analysis.

The voltage was observed to vary between levels of 685 V and 750 V, due to variations in loading and solar energy available and limited by the droop control mechanisms of the electronic components connected to the microgrid. The currents observed at the various positions were in the range between –13 A and +35 A.

Distortions have been observed with a ripple content typically below 0.8 V, equivalent to about 0.1 %, and 0.80 A for a DC current between 7 A and 21 A, equivalent to about 3.8 % maximum. This is significantly lower than the values reported in [18], which might be caused by the reduced bandwidth for the voltage sensor but is most likely also related to the higher typical power flowing in the microgrid investigated in this paper. The current ripple content at the interlink converter was significantly higher than at the PV system or EV charger, even in the case where the current was supplied by the PV system. In all measurement signals, the ripple content was higher in grid-connected mode than in islanding mode, which suggests that the interlink converter is the major source of distortions.

The maxima in the frequency spectra above 20 kHz were persistent over the whole frequency range, independent of the microgrid configuration or loading. For lower frequencies, the maxima only showed up in grid-connected mode, in line with the increased ripple content observed. Below a few hundred hertz, the distortions occurred at integer multiples of 50 Hz, suggesting they are coupled in from the AC grid through the interlink converter. Although the frequencies of the maxima for voltage and current coincide, the highest peak value for the voltage signal was observed around 113 kHz, whereas the highest peak value for the current was found around 7 kHz.

The measurement results from this work provide a useful contribution to the standardization of DC PQ measurement techniques and the development of analysis tools for DC PQ. Utilities and regulatory bodies will also benefit from the experience gained in terms of reliable planning- and compatibility-level assessments. Additional analysis of the data obtained during this measurement campaign may lead to new findings and conclusions.

## REFERENCES


[1] M. E. Baran and N. R. Mahajan, "DC distribution for industrial systems: opportunities and challenges," in *IEEE Transactions on Industry Applications*, vol. 39, no. 6, pp. 1596-1601, Nov.-Dec. 2003.

[2] T. Dragičević, X. Lu, J. C. Vasquez and J. M. Guerrero, "DC Microgrids—Part I: A Review of Control Strategies and Stabilization Techniques," in *IEEE Transactions on Power Electronics*, vol. 31, no. 7, pp. 4876-4891, July 2016.

[3] D. Kumar, F. Zare and A. Ghosh, "DC Microgrid Technology: System Architectures, AC Grid Interfaces, Grounding Schemes, Power Quality, Communication Networks, Applications, and Standardizations Aspects," in *IEEE Access*, vol. 5, pp. 12230-12256, 2017.

[4] K. Jithin, P. P. Haridev, N. Mayadevi, R. P. Harikumar and V. P. Mini, "A Review on Challenges in DC Microgrid Planning and Implementation," in *Journal of Modern Power Systems and Clean Energy*, vol. 11, no. 5, pp. 1375-1395, September 2023.

[5] M. Albu, E. Kyriakides, G. Chicco, M. Popa and A. Nechifor, "Online Monitoring of the Power Transfer in a DC Test Grid," in *IEEE Transactions on Instrumentation and Measurement*, vol. 59, no. 5, pp. 1104-1118, May 2010.

[6] M. Farhadi and O. A. Mohammed, "Real-Time Operation and Harmonic Analysis of Isolated and Non-Isolated Hybrid DC Microgrid," in *IEEE Transactions on Industry Applications*, vol. 50, no. 4, pp. 2900-2909, July-Aug. 2014.

[7] R. Weiss, L. Ott and U. Boeke, "Energy efficient low-voltage DC-grids for commercial buildings," *2015 IEEE First International Conference on DC Microgrids (ICDCM)*, Atlanta, GA, USA, 2015, pp. 154-158.

[8] IEC TR LVDC:2017-09(en), "LVDC: Electricity for the 21st Century," IEC: Geneva, Switzerland, 2017.

[9] A. Mariscotti, "Power Quality Phenomena, Standards, and Proposed Metrics for DC Grids," *Energies*, vol. 14, art. nr. 6453, 2021

[10] IEC TR 63282, "LVDC Systems–Assessment of Standard Voltages and Power Quality Requirements", IEC: Geneva, Switzerland, 2020.

[11] A. D. Femine, D. Gallo, D. Giordano, C. Landi, M. Luiso and D. Signorino, "Power Quality Assessment in Railway Traction Supply Systems," in *IEEE Transactions on Instrumentation and Measurement*, vol. 69, no. 5, pp. 2355-2366

[12] G. Cipolletta, A. D. Femine, D. Gallo, Y. Seferi, F. Fan and B. G. Stewart, "Detection of Dips, Swells and Interruptions in DC Power Network," *2022 20th International Conference on Harmonics & Quality of Power (ICHQP)*, Naples, Italy, 2022, pp. 1-6

[13] G. Cipolletta, A. D. Femine, D. Gallo, C. Landi and M. Luiso, "Considerations on Voltage Ripple Assessment in dc Power Network," *2022 IEEE 12th International Workshop on Applied Measurements for Power Systems (AMPS)*, Cagliari, Italy, 2022, pp. 1-6

[14] H. van den Brom et al., "Traceable Power Quality Measurements in DC Electricity Grids, *Proceedings of the Conference on Precision Electromagnetic Measurements*, Wellington, New Zealand, December 2022, pp. 1-2.

[15] G. Frigo and J. Braun, "Measurement Setup for a DC Power Reference for Electricity Meter Calibration," *2022 20th International Conference on Harmonics & Quality of Power (ICHQP)*, Naples, Italy, 2022, pp. 1-5.

[16] H. van den Brom, Z. Marais and R. van Leeuwen, "Testing of DC Electricity Meters with Broadband Conducted Electromagnetic Disturbances," *2022 20th International Conference on Harmonics & Quality of Power (ICHQP)*, Naples, Italy, 2022, pp. 1-6.

[17] M. A. Oliván, J. J. Pérez-Aragüés, and J. J. Melero, "A High-Frequency Digitiser System for Real-Time Analysis of DC Grids with DC and AC Power Quality Triggering," *Applied Sciences*, vol. 13, no. 6, p. 3871, Mar. 2023.

[18] H. E. van den Brom, R. van Leeuwen, G. Maroulis, S. Shah, and L. Mackay, "Power Quality Measurement Results for a Configurable Urban Low-Voltage DC Microgrid," *Energies*, vol. 16, no. 12, p. 4623, Jun. 2023.

[19] M. Blaz, J. Langemann, M. Schmidt and C. Leicht, "Setup for testing energy meters with disturbed DC signals occuring in DC charging stations," *2023 IEEE 13th International Workshop on Applied Measurements for Power Systems (AMPS)*, Bern, Switzerland, 2023, pp. 1-6.

[20] H. E. van den Brom et al., "EMC Testing of Electricity Meters Using Real-World and Artificial Current Waveforms," in *IEEE Transactions on Electromagnetic Compatibility*, vol. 63, no. 6, pp. 1865-1874, Dec. 2021.

[21] H. E. van den Brom, R. van Leeuwen and R. Hornecker, "Characterization of DC Current Sensors With AC Distortion for Railway Applications," in *IEEE Transactions on Instrumentation and Measurement*, vol. 68, no. 6, pp. 2084-2090, June 2019.